SECOND EUROPEAN ROTORCRAFT AND POWERED LIFT AIRCRAFT FORUM

Paper No 21

THE FLOW OVER A HELICOPTER BLADE TIP IN THE TRANSONIC REGIME

F.X. Caradonna
US Army Air Mobility Research and Development Laboratory (USAAMRDL)
Ames (Calif.) USA

J.J. Philippe
Office National d'Etudes et de Recherches Aérospatiales (ONERA)
92320 Châtillon (France)

September 20-22, 1976

Bückeburg, Federal Republic of Germany

Deutsche Gesellschaft für Luft- und Raumfahrt e.v.

Postfach 510645, D-5000 Köln, Germany

THE FLOW OVER A HELICOPTER BLADE TIP IN THE TRANSONIC REGIME

F.X. Caradonna
U.S. Army A.M.R.D.L. – Ames – U.S.A.

J.J. Philippe
Office National d'Etudes et de Recherches Aérospatiales (ONERA)
92320 Châtillon (France)

Summary

A combined experimental-computational investigation of transonic flow on an advancing rotor has been performed. The test model is a modified Alouette II tail rotor instrumented with absolute pressure transducers. The computational model is the two-dimensional transonic small disturbance equation. The agreement between computation and experiment is good.

The results obtained show that unsteadiness is an important part of the problem. Unsteady lifting computations indicate the possibility of loads different from those observed usually in steady flows. The computations also show a great sensitivity to angle of attack variations.

Résumé

Les écoulements transsoniques, qui apparaissent sur un rotor d'hélicoptère en vol d'avancement, ont fait l'objet d'une étude théorique et expérimentale. La maquette essayée en soufflerie est celle d'un rotor arrière Alouette II modifié et équipé de capteurs de pression absolue. Pour les calculs, l'équation des petites perturbations du potentiel des vitesses pour les écoulements bidimensionnels instationnaires a été utilisée. La comparaison entre les calculs et l'expérience est bonne.

Les résultats montrent l'importance des effets dus au fonctionnement instationnaire des profils de la pale. Des calculs instationnaires pour des profils portants indiquent la possibilité de l'existence d'efforts très différents de ceux habituellement observés en écoulement stationnaire. Ils montrent aussi une grande sensibilité aux lois de variations de l'angle d'attaque.

1 – INTRODUCTION

High speed rotor flow has been a relatively unexplored area of study because the problem is experimentally very difficult and analytically next to impossible. However, with the exception of separation (shock induced or otherwise) there is little of the flow physics which is not fairly well understood. The main roadblocks to progress in this field have been the limitations of instrumentation and mathematical analysis. Therefore, it was decided at USAAMRDL-Ames several years ago to defer the classical analysis and experiment process and concentrate rather on computational simulation of transonic rotor flow. Since then it has been found that computation can be as experimental as anything done in a wind tunnel. The uncertainties and limitations of computation are significant, but no greater than –and certainly very different from– those of tunnel testing. Neither test nor computation can stand alone ; only together do they reveal our grasp of the problem. Thus, as part of the Memorandum of Understanding between France and the United States for a Cooperative Research Project in Helicopter Dynamics, ONERA and AMRDL are conducting a joint experimental-computational investigation, some results of which are presented here.

It is well known that helicopter rotors do strange things at high tip speeds. Certainly the power losses, blade vibration and pitch link loads rise very rapidly. Paul, Ref. (1), has reported on some curious tracking difficulties and subharmonic oscillations encountered in high speed tests of a Sikorsky NH-3 compound helicopter. Similar observations on a BO 105 have been reported by Huber and Strehlow, Ref. (2). In both cases it was clear that the problem was associated with transonic flow and the phenomena could only be explained by having the proper airfoil characteristics. The point which we will make in this paper is that transonic airfoil characteristics that ignore unsteadiness may not be sufficiently accurate for rotary wing work. Early computational attacks on the problem, Refs. (3) and (4), address the important three-dimensional effects but ignore unsteadiness. That unsteadiness has not been the subject of much previous work is probably due to the lack of detailed rotor pressure observations. Probably the first indication that unsteadiness may be significant was the computational experiments of Caradonna and Isom, Ref. (5). In this work some simple non-lifting computations of a rotor in forward flight were made. These showed that there was a significant difference between quasi-steady and unsteady computations. The unsteady shocks were somewhat weaker in the first quadrant but continued to grow in the second quadrant and only after some delay did they move forward again –but with greater strength and rapidity than quasi-steady theory predicts. With this as a guideline, one would know what to look for in an experiment. That experiment is described in this paper. In addition, some two-dimensional, non-lifting computations are performed and compared with the experimental data. Some lifting computations are also made in order to determine the possibilities of unusual rotor loads.

2 – EXPERIMENTAL STUDIES ON BLADE TIP FLOWS

2.1 – Test facilities

Figure 1 shows a layout of the S2 Chalais-ONERA test stand for studying model rotors. The wind tunnel is 3 m. in diameter and has a maximum speed capability of 110 m/sec. (400 km/h). The tip path plane angle is controlled by means of shaft tilt. The maximum tip speed of the 1.5 m. diameter rotor is about 200 m/sec. Thus we can simulate tip Mach numbers approaching one and advance ratios up to 0.55.

Total rotor forces are measured by a six-component balance and rotating torquemeter located close to the hub. Data from the blade are transmitted via either a 55 or 48 channel slip ring assembly. An electro-pneumatic switching device permits the simultaneous transmission of the output of 12 transducers through the 48 channel slip ring assembly.

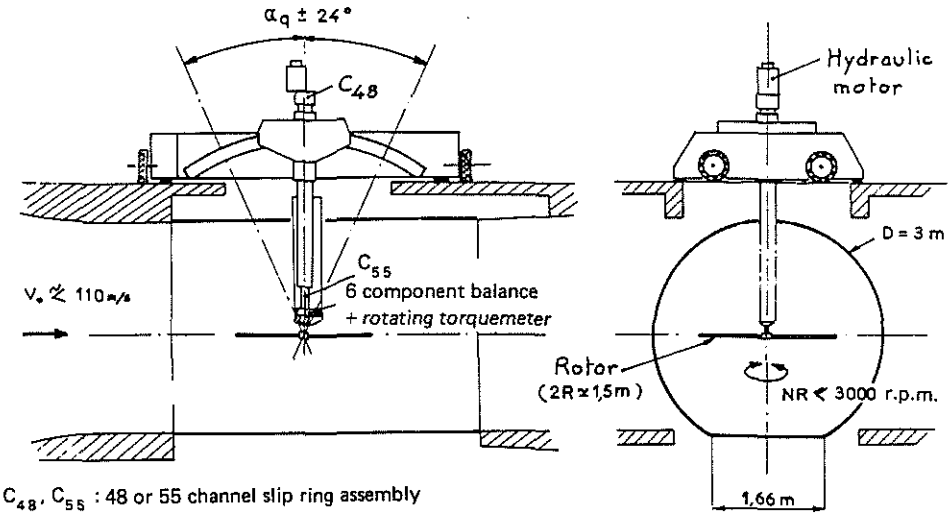

C_{48}, C_{55} : 48 or 55 channel slip ring assembly

Fig. 1 — Helicopter rotor test stand in S2 Chalais ONERA wind-tunnel.

2.2 — The rotor

Figure 2 shows the rotor with which we studied the blade tip flows. The blade is that of Alouette II tail rotor with a removable tip attached at the 0.8 radius section. The tip being of carbon epoxy construction, is very stiff and light. The profiles are symmetrical (NACA 00XX) with a thickness ratio which decreases from root to tip. Figure 3 shows a layout of the tip and gives the chordwise and spanwise locations of the various pressure ports. There are three spanwise instrumentation stations located at 0.855 R, 0.892 R and 0.946 R and having 8, 14 and 8 transducers respectively.

2.3 — The pressure transducers

The Kulite LDQL transducer, an absolute pressure transducer with acceleration compensation, was used throughout the test. The transducers are buried in the center of the blade and connected to both the top and bottom surfaces by a T-shaped tube. The top and bottom surface pressures are then obtained by obstructing one or the other of the T-tube branches. The output voltage of the transducer is about 20 mV per atmosphere with a 20 V supply voltage. Even though the transducers are coupled with a temperature compensating module, it was found necessary to accurately calibrate the device for both pressure and temperature independently. The pressure for zero output voltage is the more temperature sensitive parameter, and can reach a value of 1 mbar/°C. Temperature gauges are therefore required for temperature measurements in each spanwise station. 9 Kulite thermal sensors are used (3 per station). The rotor tip speed being about 200 m/sec, the transducer is subject to about 5000 g acceleration. The acceleration calibration was performed by running the rotor in hover with both branches of the T-tube obstructed. The pressure increase due to the air imprisoned in the T-tube is taken into account according to the local blade temperature rise due to air friction. In general, this transducer yields a response of less than 10 mbar for 5000 g and a systematic correction for acceleration is not necessary.

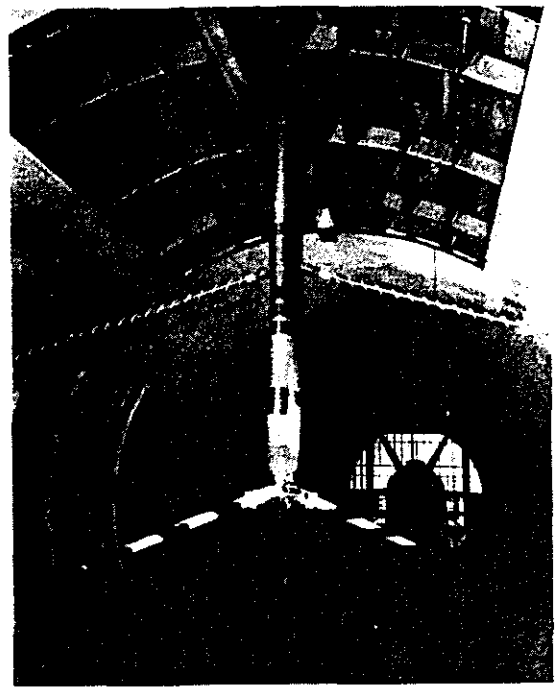

Fig. 2 — View of the rotor in the wind-tunnel.

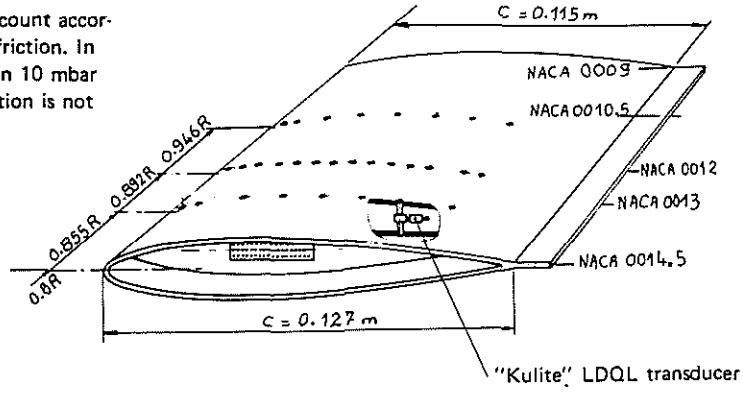

0.855 R = 5, 10, 20, 30, 40, 50, 60, 75 %

0.892 R = 5, 10, 15, 20, 25, 30, 35, 40, 45, 50, 55, 60, 65, 70, 75 %

0.946 R = 5, 10, 20, 30, 40, 50, 60, 70 %

Fig. 3 — Tapered in thickness tip layout.

2.4 — Data acquisition and processing

The data obtained on the blade are transmitted via the electro-pneumatic switch and slip rings to an amplifier. A special computer averaging device is used and allows to get n cycles of mean instantaneous values corresponding to 256 azimuthal positions of the blades. The final results are written on line on magnetic digital tape for subsequent off-line processing. An example of the results obtained from this is shown in Fig.4. Shown here is the output of two transducers located at x/c = 0.45 and 0.55 chordwise positions on the NACA 0012 section at the 0.892 R station.

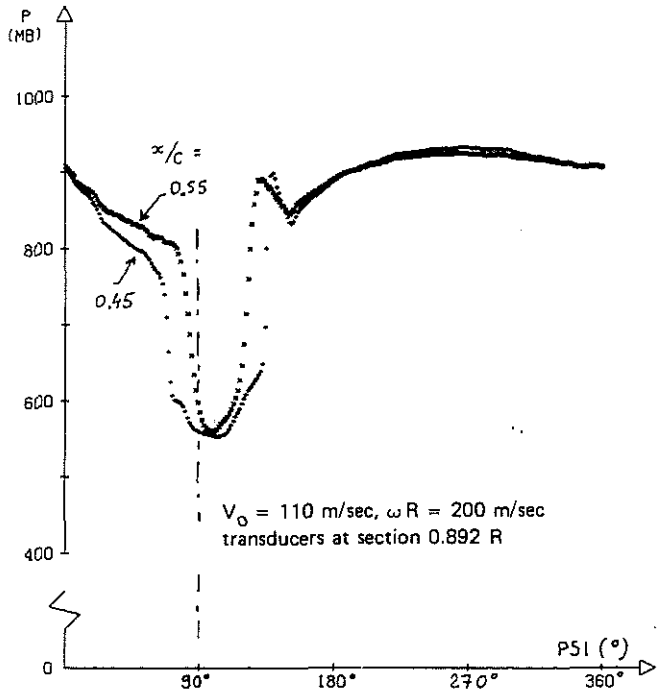

Fig. 4 — Example of results.

2.5 — Typical experimental results

Figure 5 shows typical pressure variations when the tip Mach number is high enough to have supercritical flow on the advancing blade. Here we show the case of the non-lifting rotor at 0.55 advance ratio (V_0 = 110 m/sec, ωR = 200 m/sec). Three pressure histories at different chordwise locations at 0.892 R are shown. These pressure traces show rapid breaks indicative of a shock passing over the transducer. As the blade advances from ψ = 0° to ψ = 90°, the break in the pressure trace is seen at the x/c = 0.45 chordwise location, but not at x/c = 0.25. Therefore, as the Mach number increases (local Mach number, M_ℓ = 0.530 + 0.327 Sinψ) the shock is born somewhere between these two locations. The shock is subsequently seen passing the x/c = 0.55 location. The first clear indication that this flow is truly unsteady is that the pressure trace is not symmetrical about ψ = 90°, but rather continues to expand somewhat beyond this point. This is more clearly seen in Fig. 4. The shock motion inferred from Figs. 4 and 5 is especially interesting. As the flow decelerates, in the second rotor quadrant, the shock travels upstream on the blade. However, it does not merely return to its place of origin. Rather, it continues to advance toward the leading edge and is clearly seen passing the x/c = 0.25 location in Fig. 5.

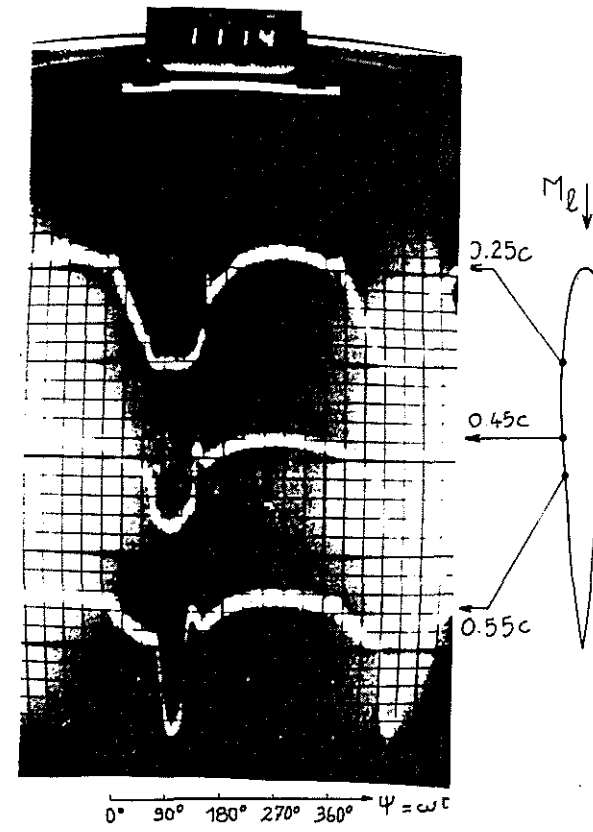

Fig. 5 — Typical pressure variations for non lifting case. NACA 0012.
μ = 0.55, V_0 = 110 m/sec, ωR = 200 m/sec, 0.892 R station, M_ℓ = 0.530 + 0.327 Sinψ.

The flow asymmetry which characterizes this unsteadiness is better seen in Fig. 6. Here the chordwise pressure distributions at the 0.892 R station are shown for azimuthal positions of ψ = 60° and 120°. If the flow were quasi-steady, the pressure distributions would be identical at these two azimuths. However, as advance ratio and Mach number increase into the supercritical region the difference between the two pressure distributions is quite marked. For a local Mach number of 0.734 the flow is slightly subcritical and the difference in the two pressure distributions is not great. At the higher Mach numbers shown the asymmetry and the forward moving shocks are unmistakable. The shocks in the decelerating flow are seen to be always stronger than that in the accelerating flow. In fact at a local Mach number of 0.759 the flow is supercritical in both the accelerating and decelerating flows. However, while the latter flow displays a sizable shock, the former still appears shockless. Above a Mach number of 0.78, which is approximately the drag divergence point for the NACA 0012 profile, the shocks are clearly seen in both the first and second quadrants.

Figure 7 shows the three-dimensional pressure distribution on the rotor for the 60° and 120° azimuth positions. At ψ = 60°, the shock is very nearly parallel to the leading edge. Furthermore, the degree of flow expansion is not very different at the three spanwise stations. So at this point the tip relief, decreasing thickness ratio and spanwise increasing local Mach number are apparently combining to produce very small spanwise gradients. At ψ = 120°, however, the supersonic expansion region becomes larger with increasing span. It would seem that the flow is more unsteady as the tip is approached. Beyond this, however, there is little we can say in the absence

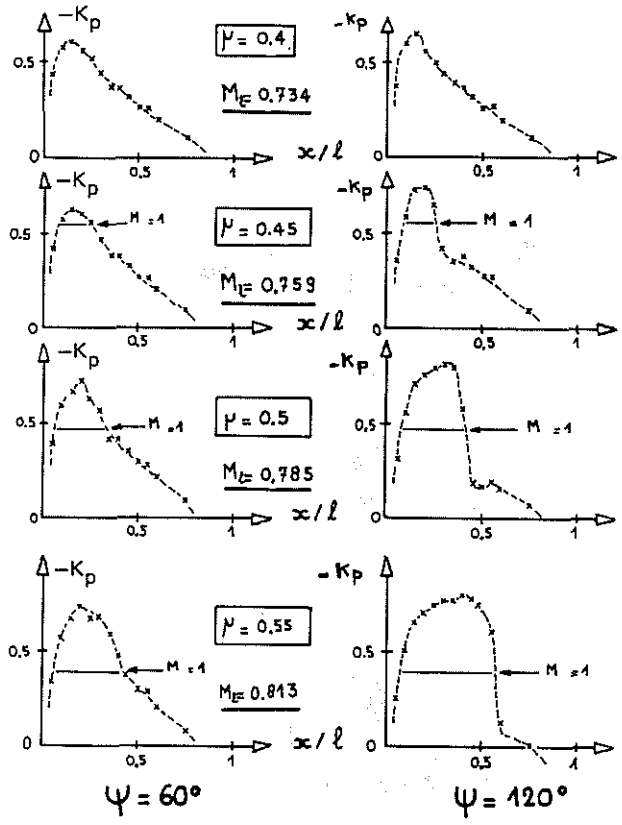

Fig. 6 — Unsteadiness effect on experimental pressure distributions. Non lifting case.

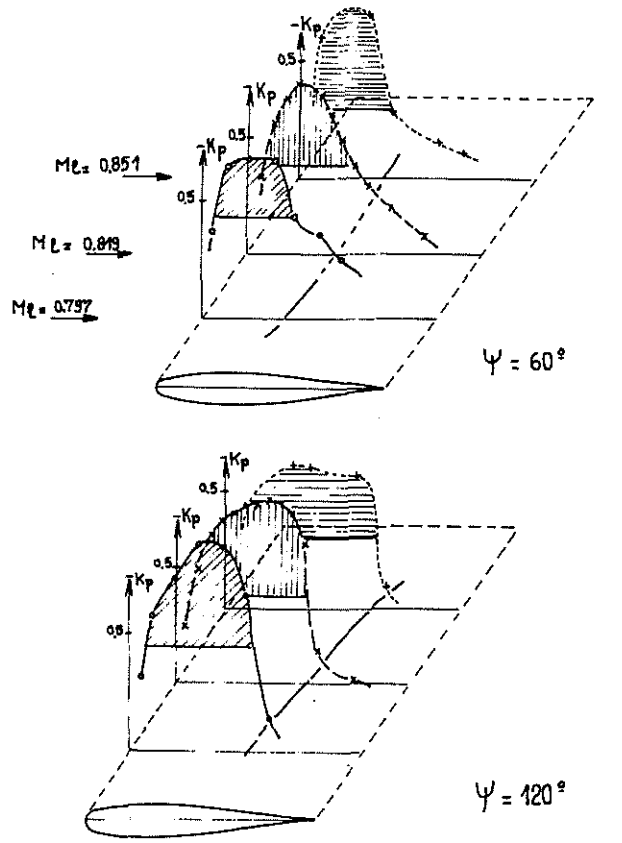

Fig. 7 — Three-dimensional pressure distribution on blade tip. Non lifting case.

of three-dimensional computations. We have, however, computed two-dimensional simulations of this flow, the results of which are shown and compared in a later section for this non-lifting case. During the wind-tunnel tests, the rotor with two untwisted blades had a mean zero lift. We observed only a very little flapping motion of each blade, which gave very few difference between top and bottom surfaces pressures on the advancing blade.

It is clear from these observations that the unsteady transonic effects first predicted in Ref. (5) are real. That is, as soon as a flow becomes supercritical, the flow upstream signal propagation rate and the embedded supersonic region combine to render the flow incapable of reacting quickly to a changing environment. The results of this for a rotor is that while the local flow is accelerating the flow is less expanded and shocks are weaker than what would occur in steady flow. The peak expansion can occur well after $\psi = 90°$. When the supercritical region does collapse, it can do so quite rapidly with shocks stronger than predicted by steady data. And these shocks can transverse very far forward on the blade.

It now remains to correlate the above observations with computations.

The pressure coefficient C_p (or K_p) is defined by :

$$C_p \text{ (or } K_p) = \frac{p - p_o}{1/2\,\gamma\, M_\ell^2\, p_o}$$

and, then, is referred to the instantaneous incident Mach number M_ℓ, normal to the leading-edge of the blade.

3 — COMPUTATIONAL STUDIES OF BLADE TIP FLOWS

3.1 — The governing equation

The flow is assumed to be inviscid and irrotational. Therefore, a potential formulation will be valid for flows not having excessive shock strengths. For present purposes the flow is assumed to be two-dimensional (sweep effects and tip relief are ignored). A blade section at a distance, r, from the center of rotation sees a sinusoidally varying incident velocity.

$$v = \omega r + V_o \sin\psi$$

The incident Mach number at this point is then

$$M_\ell = M_r\,(1 + \mu' \sin\psi)$$

where M_r is the rotational Mach number, $M_r = \omega r/a_o$, a_o is the undisturbed sound speed, $\mu' = V_o/\omega r$ (the local advance ratio) and $\psi = \omega t$, the azimuth angle. The transonic small disturbance potential equation for a blade section seeing the above Mach number variation is :

$$(1) \qquad A\,\phi_{\psi\psi} + B\,\phi_{x\psi} = C\,\phi_{xx} + \phi_{yy}$$

where $A = \dfrac{M_r^2}{\lambda'^2 \delta^{2/3}}$, $B = \dfrac{2 M_r^2}{\lambda' \delta^{2/3}}(1 + \mu' \sin\psi)$

$$C = \left[\frac{1 - M_r^2 (1+\mu'\sin\psi)^2}{\delta^{2/3}} - \frac{(\gamma-1)}{\lambda'} M_r^2\,\phi_\psi \right.$$

$$\left. - (1+\gamma) M_r^2 (1+\mu'\sin\psi)\,\phi_x \right]$$

δ = blade thickness ratio, $\lambda' = r/c$ (a local aspect ratio), $x = \bar{x}/c$, $y = \delta^{1/3}\,\bar{y}/c$ and $\phi = \Phi/\omega r c \delta^{2/3}$. $\bar{x}$ and $\bar{y}$ are the physical chordwise and normal coordinates respectively and Φ is the full velocity potential. (The complete derivation of this equation is found in Ref. (6)). In this equation the inverse of the aspect ratio appears as a reduced frequency. It is the nonlinear coefficient, C, which models the mixed supersonic-subsonic

nature of the flow and allows the existence of shocks in the computation. If unsteadiness is assumed to be solely due to the sinusoidally varying Mach number and to a similar angle of attack variation, the reduced frequency of motion is of the order of $1/\lambda'$ and the second time derivative term $\phi_{\psi\psi}$ and the term ϕ_{ψ} in C are negligible. In fact, these terms could easily become significant if wake effects were considered, but this is not done at this time. The boundary conditions on the body are :

$$\phi_y(X, 0^{\pm}) = T'(X) \pm \alpha/\delta \tag{2}$$

where T' is the normalized body slope and α is the angle of attack. The far field boundary potential is assumed to be that due to a point vortex

$$\phi(X,Y) = -\frac{[\phi]_{TE}}{2\pi} \tan^{-1}\left(\frac{\sqrt{1-M_\infty^2}}{\delta^{1/3}} \frac{Y}{X}\right) \tag{3}$$

where $[\phi]_{TE}$ is the potential discontinuity at the trailing edge. This latter boundary condition is undoubtedly incorrect as it does not properly consider thickness and retarded time effects. However, due to the large distance of the boundary from the airfoil, this has been found to be of little consequence. The Kutta condition is enforced by setting the potential discontinuity behind the airfoil equal to that at the trailing edge at the previous time step (or iteration) and calculating the far field potential using eq. (3).

3.2 — The numerical solution

Equation (1) is a non-linear partial differential equation, which is solved by approximating the derivatives by differences at the nodes of a grid. In Ref. (5) this differencing was done in a completely implicit manner. This differencing yields a system of non-linear algebraic equations which can only be solved iteratively —originally successive overrelaxation (SOR) was used. Adams and Vander Roest, Ref. (7), subsequently adapted the Douglas-Gunn ADI (alternating direction implicit) method, Ref. (8), to solve the same difference equation. This scheme has no time step stability restrictions. Nevertheless, it is still rather inefficient because of the slow convergence rate. Ballhaus and Steger, Ref. (9), have vastly improved on this by performing a timewise linearization of the equations before solving using two methods —one of which is ADI. There is for this case a time step stability restriction, the requirement being that a shock not advance more than one mesh increment per time step. This is a very mild restriction. A stronger restriction is that the Kutta condition will not be satisfied if the time step is too large. For the iterative ADI scheme, however, the Kutta condition does not depend on time step size. A scheme which seems to work well is to use the linearized ADI for a first approximation and to subsequently perform two corrections on this using the iterative scheme. This hybrid scheme can tolerate time steps several time larger than for the linearized scheme alone and is therefore quite efficient (see appendix).

A typical rotor calculation is initiated with a steady solution computed at a point where the flow is entirely subsonic and hence quasi-steady. This initial steady solution is done iteratively and for the hybrid ADI scheme it presently accounts for much of the total running time. The time step currently used is about one degree of azimuth. At present a computation having 360 time steps requires about five minutes on a CDC 7600. So with a more efficient steady starting solution, the method is very rapid indeed.

Currently we are using three methods, SOR, iterative ADI, and the hybrid ADI scheme. Most of the results to be shown have been computed using all three approaches. The results have been nearly identical ; although the last method is by far the most efficient.

3,3 — Theoretical pressure history in the non-lifting case

Computed pressure variations for the non-lifting NACA 0012 profile in a sinusoidally varying free stream (M_∞ = 0.536 + 0.327 Sinψ) are given in Fig. 8. We consider two points (x/c = 0.3 and 0.5) on the surface. Figure 9 shows the entire chordwise pressure distribution for several of the azimuthal points in Fig. 8. From these we again observe the following typical events :

1) ψ = 50°, M_∞= 0.79 — The slope of the pressure trace steepens at x/c = 0.3 as supercritical flow commences — the steepening is not seen at x/c = 0.5 which is not yet within the short supersonic "bubble". As yet there is no shock.

2) Between ψ = 50° and ψ = 71.5° a shock has developed ahead of the x/c = 0.5 point. As the shock passes this point a precipitous break in the pressure trace is seen.

3) ψ = 90°, M_∞= 0.863 — At this time the shock is still moving rearward. Both points, being now in the supersonic region, are well expanded. At x/c = 0.3 the pressure remains almost the same, while at x/c = 0.5 the pressure is decreasing.

4) For ψ greater than 90°, M_∞ decreases and the shock wave (after some delay) moves forward. At ψ = 130° the shock is back at x/c = 0.5 and the pressure trace shows a rapid rise. At x/c = 0.3 the pressure ahead of the oncoming shock is seen now to decrease. The incident Mach number is equal to that for ψ = 50°. The difference in the pressure distribution at ψ = 50° and ψ = 130° are due solely to the time derivative terms in Eq. (1) and their importance is clearly seen.

5) At ψ = 143°, the shock is at x/c = 0.3. At x/c = 0.5, behind the shock, the flow is subsonic and re-expanding.

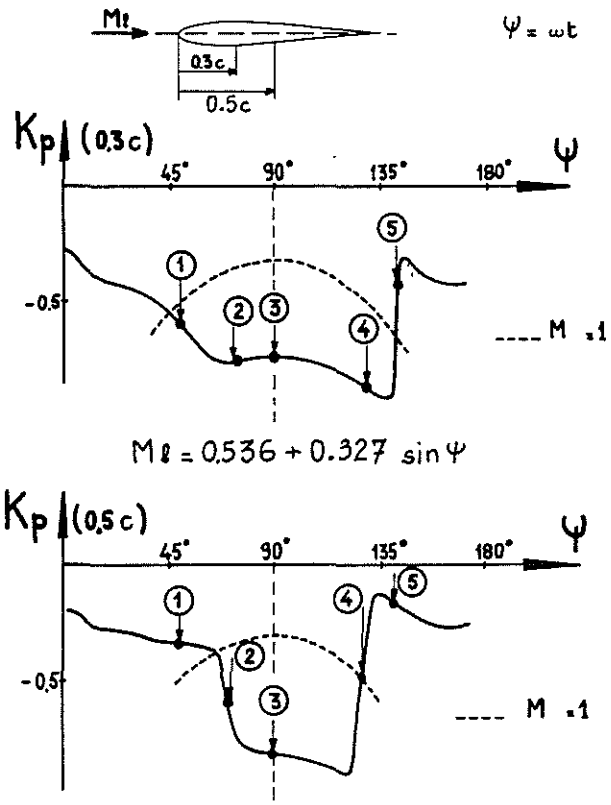

Fig. 8 — Theoretical pressure history in the lifting case.

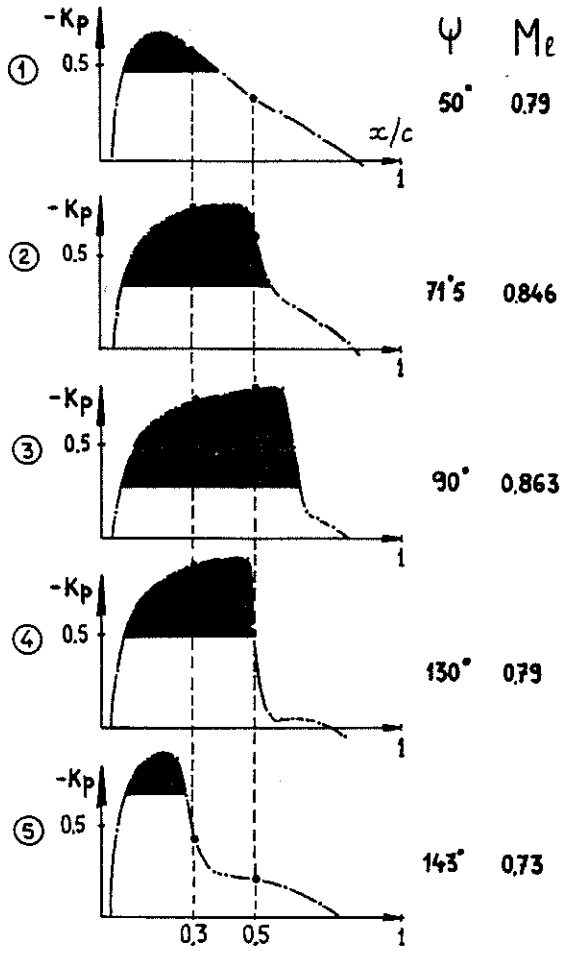

Fig. 9 — Theoretical time evolution of pressure distribution.

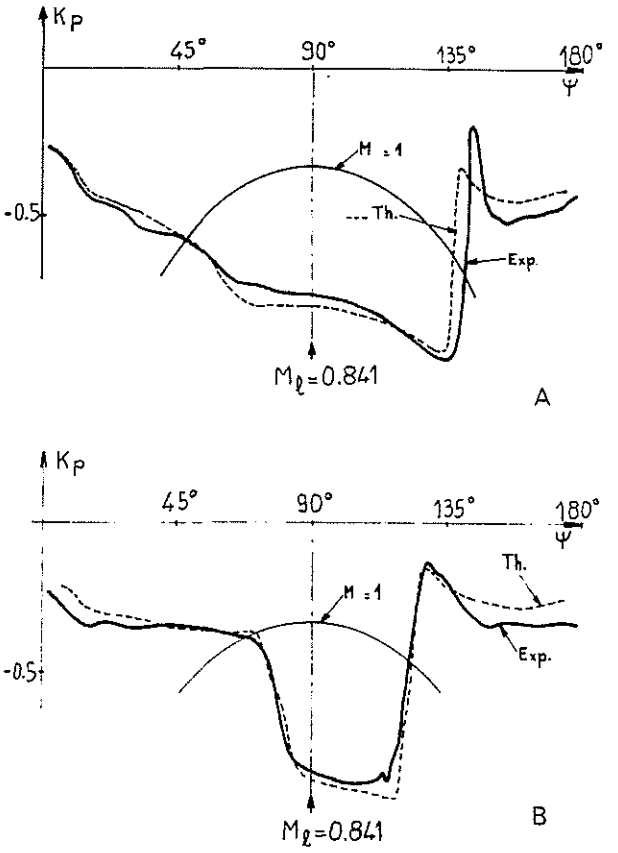

Fig. 10 — Computed and measured pressures, non lifting case, NACA 0013, r/R = 0.855, V_o = 110 m/sec, ωR = 200 m/sec.

A — x/c = 0.30 B — x/c = 0.50

3.4 — Comparison between theory and experiment

Figures 10 A and B show the comparison between computed and measured pressure variations at two chordwise locations at the 0.855 R span station. At this point the airfoil is a NACA 0013 profile. The agreement for the pressure level and shock location in time is very good. Figures 11 A and B represent the corresponding pressure variations for the 0.892 R station, where the profile is a NACA 0012. Again, the agreement is good. The differences which are seen ahead and behind the shock are probably due to a combination of viscous effects in the experiment and an inadequate number of computational points near the shock. For the 0.892 R station, Fig. 12 shows the computed and measured chordwise pressure distributions at ψ = 60° and 120° (that is, azimuths symmetrically located with respect to ψ = 90°). The timewise flow asymmetry is evident. In this figure it is seen that the observed flow is less expanded and the shock located further upstream than in the computations. This sort of difference often occurs in steady case and is usually accounted for by the inclusion of the boundary layer in the analysis.

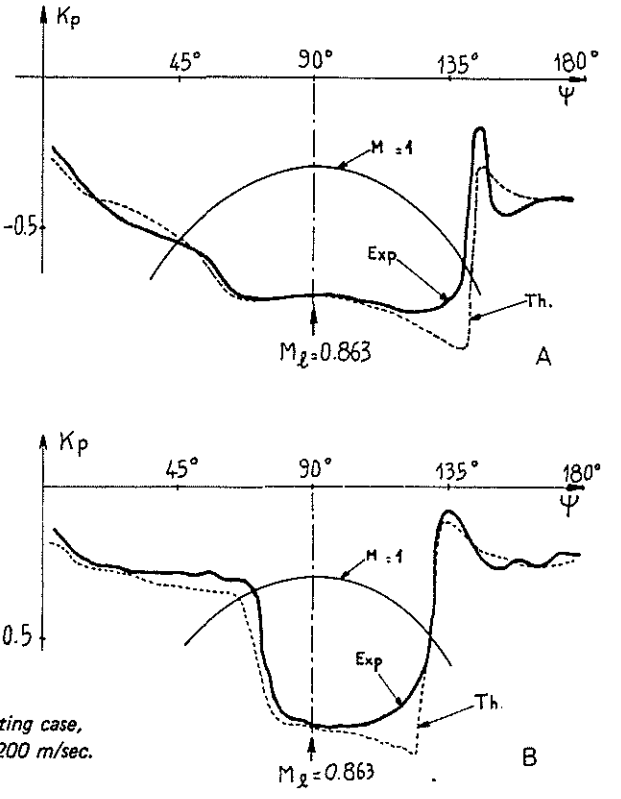

Fig. 11 — Computed and measured pressures, non lifting case, NACA 0012, r/R = 0.892, V_o = 110 m/sec, ωR = 200 m/sec.

A — x/c = 0.30 B — x/c = 0.50.

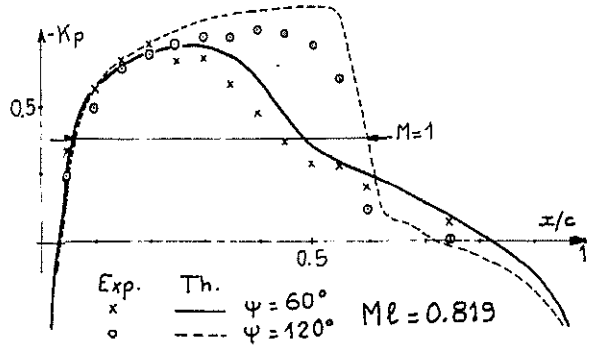

Fig. 12 — Computed and measured pressure distribution, non lifting case, NACA 0012, r/R = 0.892, V_0 = 110 m/sec, ωR = 200 m/sec.

In Figure 13 the measured and computed pressure variations are compared at 0.946 R and here the comparison is not good. This is certainly to be expected so near the tip where three-dimensional effects dominate the flow. The need for a three-dimensional extension of the above work is evident. However, it is most interesting that a transonic strip theory seems to work as well as is seen here.

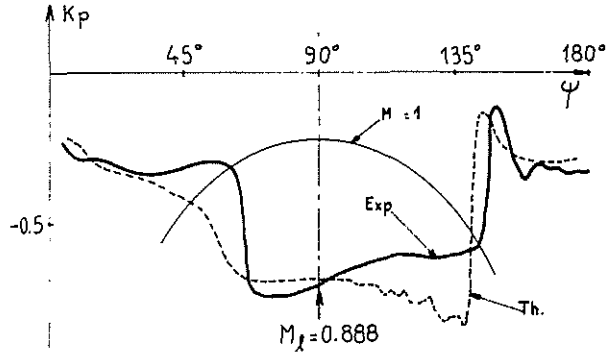

Fig. 13 — Computed and measured pressures, non lifting case, NACA 0010.5, x/c = 0.40, r/R = 0.946, V_0 = 110 m/sec, ωR = 200 m/sec.

3.5 — Application to the lifting case

To approach the more realistic problems concerning the lifting rotor we must know the angle of attack variations for a given blade section. Various types of methods can be used to evaluate it. Here, to simplify matters, we will assume a pure sinusoidal variation of the angle of attack, which is quite realistic for the advancing blade.

Consider a rotor with a NACA 0012 airfoil. Assume an advance ratio of 0.25, an aspect ratio of 13.7 and an advancing tip Mach number of 0.906. (These numbers are chosen as being typical of some current production machines). We shall compute the flow at the 0.925 R station using the two-dimensional flow assumption. (At this point the local Mach number variation is $M_\ell = 0.661 + 0.179 \sin\psi$).

We will consider three cases of sinusoidal variation of the angle of attack, giving a negative value (first case), a zero value (second case), and a positive value (third case) for the advancing blade $\psi = 90°$.

Figure 14 shows the load variation on this section when the angle of attack is assumed to vary sinusoidally from 6° at $\psi = 270°$ to −0.5° at $\psi = 90°$ (First case). The most obvious effect of unsteadiness here is that the point of maximum negative lift occurs well beyond the 90° azimuth position. The lift is similar at $\psi = 0°$ and 180° indicating that at these points the flow is not far from being quasi-steady. The rapidity with which the lift switches from negative to positive values is interesting. This is because the bottom surface flow is slow to respond to the decelerating free stream and increasing angle of attack. It finally does respond with a very rapid forward motion of the lower surface shock. This shock motion is so rapid that the shock gives the impression of leaving the airfoil entirely. It is seen in Fig. 14 that when the shock approaches the leading edge a small nose-down moment is produced. And just beyond this point the weak shock (or at least the remnant of a shock) is clearly seen near the leading edge on the lower surface.

For the second case of an angle of attack which goes to zero at $\psi = 90°$, Fig. (15), it is clearly seen that not only does the point of minimal lift occur well after 90°, but the lift does not go to zero. Also the moment variation is much less than the previous case.

Fig. 16 shows the third case where the angle of attack goes to +0.5° at 90° azimuth. In this case there occurs a large lift overshoot in the second quadrant. This is because there is a considerable difference in the size of the supersonic regions on the top and bottom surfaces of the airfoil. The upper surface flow being much more supercritical is far slower to respond to changing conditions than the lower surface flow. Furthermore, the increasing angle of attack now lessens the effect of decreasing Mach number in forcing the upper surface flow to a less expanded state. On the bottom surface the effects of decreasing free stream Mach number and increasing angle of attack both combine to decrease the flow expansion, but in this case the barely supercritical flow is much quicker to respond. The result of this difference in flow response on the top and bottom surface is the lift overshoot. In all these cases the effect of unsteadiness is to shift the maximum loading into the second quadrant and to increase the lifts obtained. In the last case shown, this lift increase is quite dramatic and in no way similar to anything that might occur in steady theory.

Figure 17 shows comparisons of forces and moments computed with quasi-steady or unsteady equations. It is seen here that the unsteady lift is generally more positive than steady theory predicts —and the moments are weaker—. The phase-lag for maximum C_M or for minimum C_N is also clearly shown in the unsteady case.

The effect of Mach number on unsteadiness is seen in Fig. 18 which shows the lift and moment variation for a range of tip speeds. In this case the angle of attack goes to −0.5° at $\psi = 90°$. At a tip Mach number of 0.863 there is little asymmetry about the $\psi = 90°$ point. Increasing Mach number is seen to increase the loads and shift the point of maximum load further and further beyond $\psi = 90°$. However, all these load variations are qualitatively similar.

For the case of $\alpha = 0°$ at $\psi = 90°$ (Fig. 19) the increase in tip Mach number from 0.863 to 0.906 shows an expected increase in minimum lift and a shift in this point beyond $\psi = 90°$. However, at a Mach number of 0.928 the lift overshoot is seen to occur. The high Mach number cases in Figs. 18 and 19 show very different load variations and yet the difference between them is only 0.5° in angle of attack. Such an extreme sensitivity to angle of attack variation is starting. It should be remembered that even steady transonic flows are very sensitive to angle of attack —but not quite to the extent which we see here.

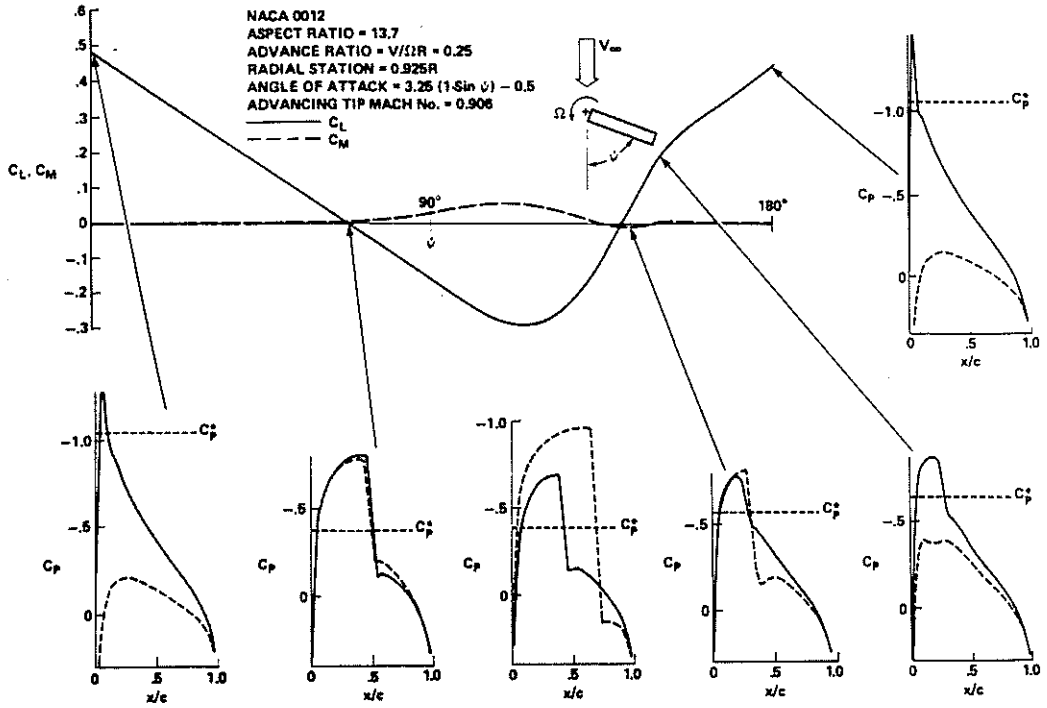

Fig. 14 — Load variation on a helicopter rotor (first case).

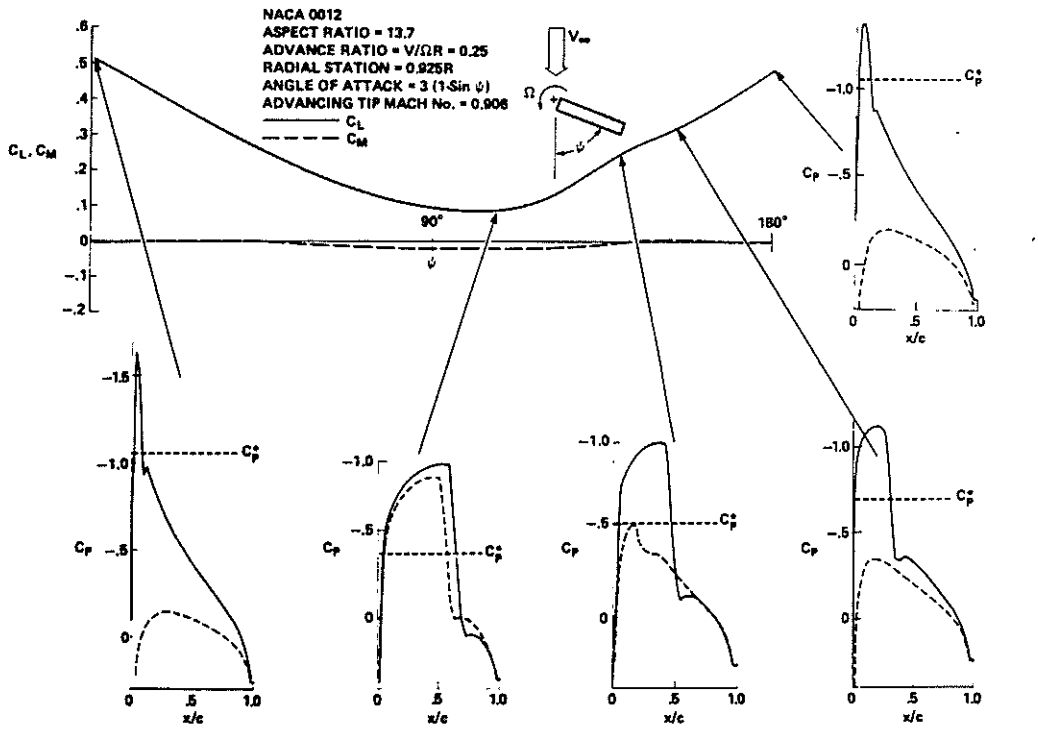

Fig. 15 — Load variation on a helicopter rotor (second case).

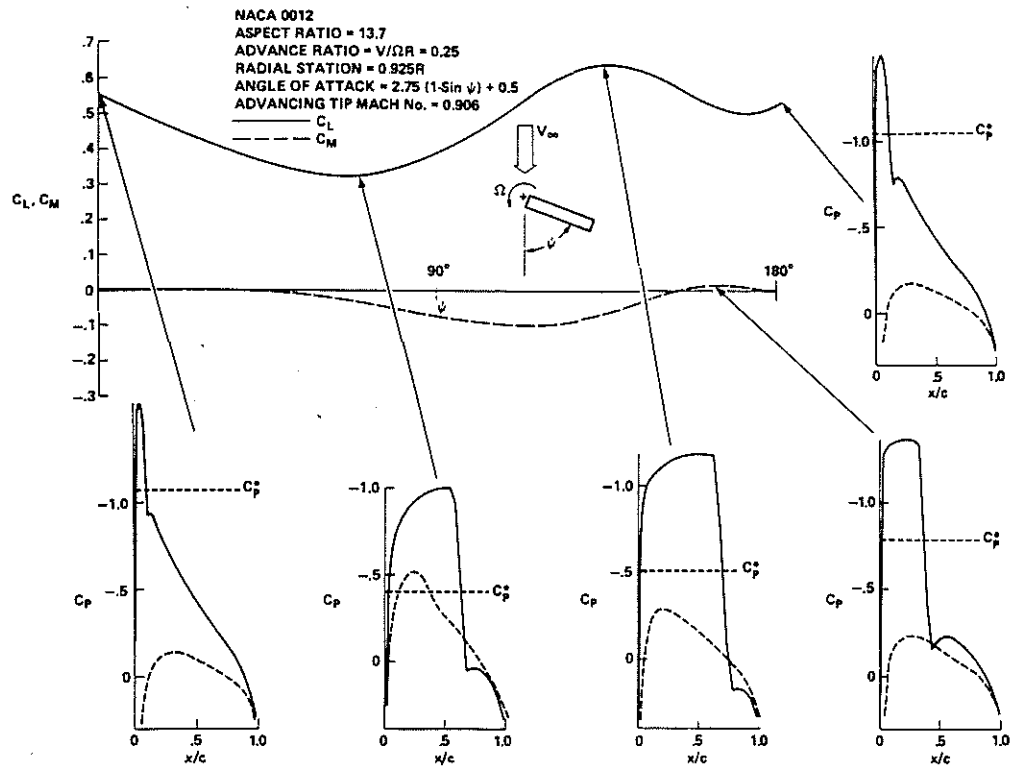

Fig. 16 — Load variation on a helicopter rotor (third case).

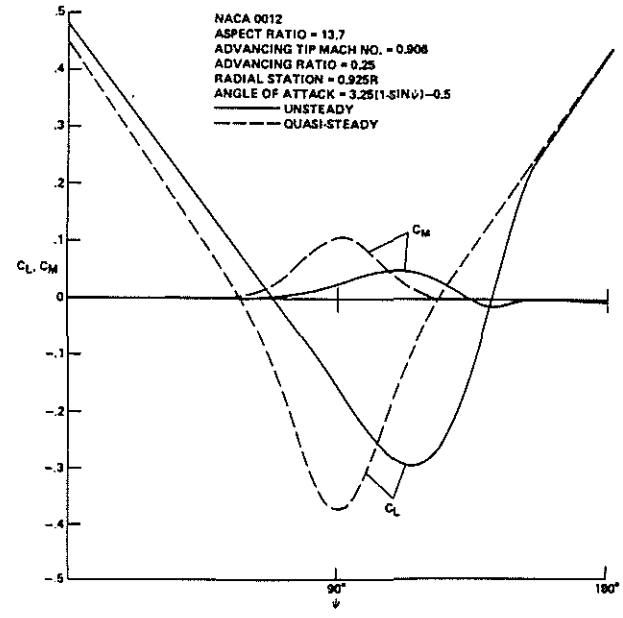

Fig. 17 — Comparison of computed unsteady and quasi-steady rotor blades.

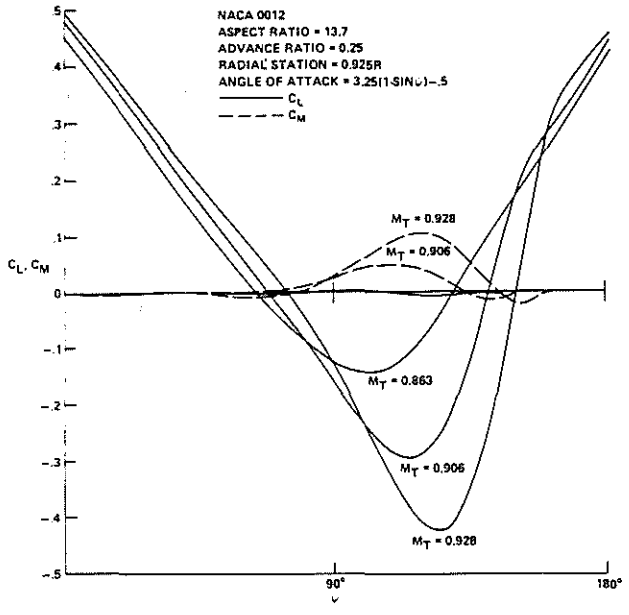

Fig. 18 – Lift and moment variation v.s. advancing tip Mach number (first case).

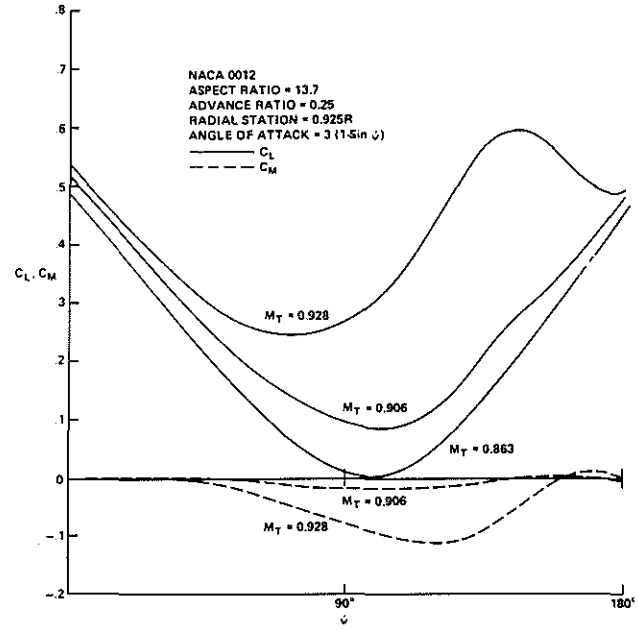

Fig. 19 – Lift and moment variation v.s. advancing tip Mach number (second case).

It cannot be said that the above types of loading occur in any particular rotor. Clearly the great sensitivity of the loads to the angle of attack calls into question the applicability of any assumed blade incidence history. What must be done in the future is to couple the above method with a good rotor downwash prediction method and a blade elasticity program. This task does appear to be within the capabilities of our fastest computer.

4 – CONCLUDING REMARKS

The combined experimental and theoretical studies presented herein show :

– unsteadiness is a major and unmistakable feature of transonic rotor flow ;

– non-lifting comparisons with experiment indicate that major features of this flow can be readily and cheaply predicted using current potential flow methods ;

– computational experiments reveal a real possibility of some rather unusual loading effects at high advancing tip Mach number.

It is surprising that a two-dimensional analysis should work as well as is currently indicated. At this stage of this work we should restrain our optimism, as it can remain some uncertainties of both computation and experiment. But it does seem that the small disturbance potential model captures some of the essential physics of the problem.

Future extensions of this work will require :

– Extension to three dimensions. This extension may provide a true design and optimization tool for rotor design. Some progress has already been made in this direction. However, the lifting case will be very difficult because of wake effects.

– Model testing should now be extended to lifting cases in order to determine the true loads which a rotor will see at high speed.

– The current two-dimensional code probably can and should be coupled with rotor downwash prediction and blade elasticity codes to provide a guide for present rotor design work.

– An assesment should be made of viscous effects in this flow regime.

In conclusion, it seems that, through this study, the important unsteady transonic phenomena on advancing blade can be now better understood and it could help to see what are the true performance limitations of the pure helicopter. But a lot of work remains to be done, in order that a new advance may be made in the difficult problem of predicting the loads and performance of high speed helicopters. This should encourage others in rotary-wing work to join in this attractive research.

References

1. W.F. Paul, "A Self-Excited Rotor Blade Oscillation at High Subsonic Mach Number", 29th Annual National Forum –American Helicopter Society– Paper No 228, May 1968.

2. H. Huber and H. Strehlow, "Hingeless Rotor Dynamics in High Speed Flight", presented at First European Rotorcraft and Powered Lift Aircraft Forum. 22-23 September, 1975.

3. F.X. Caradonna and M.P. Isom, "Subsonic and Transonic Potential Flow Over Helicopter Rotor Blades", AIAA Journal, Vol. 10, No 12, December 1972.

4. W.F. Ballhaus and F.X. Caradonna, "The Effect of Planform Shape on the Transonic Flow Past Rotor Tips", AGARD Conf. Proc. on Aerodynamics of Rotary Wings", No 111, February 1973.

5. F.X. Caradonna and M.P. Isom, "Numerical Calculation of Unsteady Transonic Potential Flow Over Helicopter Rotor Blades", AIAA Journal, Vol. 14, No 4, April 1976.

6. M.P. Isom, "Unsteady Subsonic and Transonic Potential Flow Over Helicopter Rotor Blades", NASA CR-2463, Octob. 1974.

7. D.C. Adams and G. Vander Roest, "Iterative Solution of the Transonic Potential Equation", presented at the 1976 Army Numerical Analysis and Computers Conference, Durham, NC, February 1976.

8. J. Douglas and J. Gunn, "A General Formulation of Alternating Direction Methods," Numer. Math., Vol. 6, p. 426.

9. W.F. Ballhaus and J.L. Steger, "Implicit Approximate-Factorization Schemes for the Low-Frequency Transonic Equation, NASA TM X-73, 082, November 1975.

Appendix

In Ref. (5), Eq. (1) was differenced according to the scheme

$$(4)\quad A\delta_{\psi\psi}\phi_{i,j}^{n+1} + B^{n+1}\delta_{x\psi} = D_x f_{i,j}^{n+1} + \delta_{yy}\phi_{i,j}^{n+1}$$

where for a uniform mesh

$$\delta_{\psi\psi}\phi^{n+1} = \frac{\phi^{n+1} - 2\phi^{n} + \phi^{n-1}}{\Delta\psi^2}$$

$$\delta_{x\psi}\phi_{i,j}^{n+1} = \frac{\phi_{i,j}^{n+1} - \phi_{i-1,j}^{n+1} - \phi_{i,j}^{n} + \phi_{i-1,j}^{n}}{\Delta X\,\Delta\psi},$$

$$\delta_{yy}\phi_{i,j}^{n+1} = \frac{\phi_{i,j+1}^{n+1} - 2\phi_{i,j}^{n+1} + \phi_{i,j-1}^{n+1}}{\Delta y^2}$$

$$f_{i,j}^{n+1} = \frac{1 - M_r^2(1+\mu'\sin\psi)^2}{\delta^{2/3}} - \frac{(1+\gamma)M_r^2(1+\mu'\sin\psi)x}{2}$$

$$\frac{(\phi_{i+1,j}^{n+1} - \phi_{i,j}^{n+1})}{\Delta X} \quad (\text{a flux term})$$

D_x is a combined backward and central differenced operator which maintains flux conservation

$$D_x = \frac{1}{\Delta X}\left[(1-\epsilon_i)(f_{i,j} - f_{i-1,j}) + \epsilon_{i-1}(f_{i-1} - f_{i-2})_j\right]$$

$$\epsilon_i = \begin{cases} 0 \text{ for } C_i > 0 \quad (\text{a subsonic point}) \\ 1 \text{ for } C_i < 0 \quad (\text{a supersonic point}) \end{cases}$$

and C_i is a discretization of the non-linear coefficient

$$C_i = \frac{1 - M_r^2(1+\mu'\sin\psi)^2}{\delta^{2/3}} - (1+\gamma)M_r^2(1+\mu'\sin\psi)\,x\,\frac{(\phi_{i+1,j} - \phi_{i-1,j})}{2\Delta X}$$

In Ref. (9), Ballhaus and Steger linearize the flux expression in time. In this approach the flux is averaged at two time levels.

$$\overline{f}_{i,j} = \frac{1}{2}\left[f_{i,j}^{n+1} + f_{i,j}^{n}\right]$$

f^{n+1} is then expressed in terms of the previous time levels using a Taylor series expansion

$$f_{i,j}^{n+1} = f_{i,j}^{n} + \left(\frac{\partial f}{\partial \phi_x}\right)_{i,j}^{n}\left(\phi_x^{n+1} - \phi_x^{n}\right)_{i,j} + \cdots$$

which yields

$$(5)\quad \overline{f}_{i,j}^{n+1} = \frac{1}{2}\left\{\left[\frac{1 - M_r^2(1+\mu'\sin\psi)^2}{\delta^{2/3}} - (1+\gamma)M_r^2(1+\mu'\sin\psi)\phi_x^{n}\right]\phi_x^{n+1} + \left(\frac{1 - M_r^2(1+\mu'\sin\psi)^2}{\delta^{2/3}}\right)\phi_x^{n}\right\}$$

where for uniform mesh ϕ_x is discretized as

$$\phi_x = \frac{\phi_{i+1} - \phi_i}{\Delta X}$$

Using this flux expression in Eq. (4) and solving using the ADI scheme results in an extremely efficient algorithm.